Title

Simulations of Two-dimensional Infrared and Stimulated Resonance Raman Spectra of Photoactive Yellow Protein.

Authors

Preketes, Nicholas
Biggs, Jason
Ren, Hao
et al.

Publication Date

2013-08-01

DOI

10.1016/j.chemphys.2012.09.002

Peer reviewed

Published in final edited form as:
Chem Phys. 2013 August 1; 422: . doi:10.1016/j.chemphys.2012.09.002.

Simulations of Two-dimensional Infrared and Stimulated Resonance Raman Spectra of Photoactive Yellow Protein

Nicholas K Preketes[*], **Jason D Biggs**, **Hao Ren**, **Ioan Andricioaei**, and **Shaul Mukamel**

Abstract

We present simulations of one and two-dimensional infrared (2DIR) and stimulated resonance Raman (SRR) spectra of the dark state (pG) and early red-shifted intermediate (pR) of photoactive yellow protein (PYP). Shifts in the amide I and Glu46 COOH stretching bands distinguish between pG and pR in the IR absorption and 2DIR spectra. The one-dimensional SRR spectra are similar to the spontaneous RR spectra. The two-dimensional SRR spectra show large changes in cross peaks involving the C=O stretch of the two species and are more sensitive to the chromophore structure than 2DIR spectra.

1. Introduction

The reaction to light in all biological organisms is governed by photoreceptor proteins, which transduce light into a usable chemical signal to initiate light perception in bacteria, plants, and animals [1, 2]. The initial events in photoreceptors often involve a cis-trans isomerization in an embedded chromophore followed by a local relaxation occurring on ns timescales. Characterizing the initial events in photoreceptors is challenging because both high structural resolution and ultrafast time resolution are required [3]. Time-resolved vibrational spectroscopy is an ideal probe beacuase it provides excellent temporal and structural resolution [3, 4].

Predicting local active site motions in photoreceptors through vibrational spectroscopy could help further the understanding of the initial events in a wide range of photoreceptors existing in bacteria, plants, and animals. Photoactive yellow protein (PYP) is a 125 residue, 14 kD, globular protein with an α/β fold that is proposed to initiate the negative phototactic response in *Halorhodospira Halophila* [3, 2]. *p*-coumaric acid (pCA), the chromophore within one of PYP's two hydrophobic cores, is covalently bound to Cys69 by a thioester linkage and is stabilized by a hydrogen bond network with Glu46, Glu42, Thr50, and Cys69 [5, 3, 2].

Upon absorption (λ_{max}=446 nm), PYP undergoes a complex photocycle that was initially characterized by UV/visible absorption [6], and subsequently by time-resolved X-ray crystallography [7, 8, 9, 10, 11]. In the dark state (pG or I_0), pCA exists in the deprotonated trans form with a hydrogen bond to the amide group of Cys69 [12, 5]. After excitation, the chromophore undergoes a fs trans to cis isomerization via a bicycle pedal mechanism that

[*]Corresponding Author: Department of Chemistry, University of California, Irvine Irvine, CA 92697-2025. Phone: +001-949-824-6164 Fax +001-949-8571, nkp@uci.edu.

disrupts the hydrogen bond between pCA and Cys69 [3, 11]. Within several nanoseconds, relaxation around the active site leads to the formation of the red-shifted intermediate (pR or I_1) [13, 8, 10, 11]. The chromophore is then protonated by Glu46 [13, 14], causing a protein quake that partially unfolds it [7, 15] on a millisecond timescale to form its putative signaling state (pB or I_2). Finally, in a subsecond process, the pG state is recovered. This involves the deprotonation of pCA by Glu46, the reisomerization of pCA, and the refolding of the protein [3].

The isomerization follows a “volume-conserving” path because the chromophore is embedded within the densely packed hydrophobic core [13, 8, 11]. The strong hydrogen bonding network and the covalent attachment to Cys69 further constrain the number of such mechanisms [16]. The trans to cis isomerization is achieved via a bicycle pedal mechanism where the rotation about the double bond is concomitant with a rotation about the C-C(=O) bond. This breaks the hydrogen bond between Cys69 and pCA, shifting the pCA carbonyl stretch from 1633 to 1666 cm^{-1}[17]. Following this bicycle pedal mechanism, rotations about the S-C(=O), C^{α}-C^{β}, and C^{β}-S bonds leads to the formation of pR by relieving strain in the active site [13, 8, 16, 10, 11].

Both Infrared (IR) and resonance Raman (RR) spectroscopy detect vibrational resonances, but through a different window. In RR, only those vibrations which are coupled to an excited state are observed, which permits the observation of vibrational dynamics of a chromophore within a host. This site selectivity has been used to study photosensors such as rhodopsins and phytochromes. On the other hand, IR spectroscopy observes all vibrational resonances within the pulse bandwidth. The secondary structure of proteins is observed via the amide transitions. However, if a small number of vibrational resonances are spectrally isolated (e.g. by isotope labeling), IR spectra may also be used to study local dynamics.

In this paper, we report simulations of IR and RR spectra of the pG and pR states of PYP. Details of the quantum chemical and molecular dynamics simulations are given in section II. The simulated IR spectra are presented in section III and compared with experiment. We particularly focus on the IR difference spectrum of the Glu46 COOH stretch. We also present the simulated 2D IR spectra for pG and pR. In section IV, the simulated spontaneous RR spectra are presented and compared with experiment. The simulated one and two-dimensional stimulated RR spectra are presented as well. We finally conclude and discuss future extensions.

2. Methods

2.1. Molecular Dynamics Simulations

Molecular dynamics (MD) simulations of the pG and pR states of PYP were performed using the GROMACS software package [18]. The pG initial structure was taken from PDB 1NWZ [9] and the pR initial structure was taken from PDB 1OT9 [10]. The protein was modeled using the Gromos96 united-atom force field [19] and the parameters for PCA were obtained from a previous study [20].

Each structure was solvated in a cubic box of SPC water [21] with a minimum solvation layer of 0.9 nm. This resulted in a box of length 62.7 Å for pG and 63.4 Å for pR. To neutralize the system, six water molecules were replaced with sodium ions. The systems were minimized for 5000 steps using a steepest descent algorithm. The water, ions, and protein hydrogens were then allowed to relax for 250 ps in the NPT ensemble while non-hydrogen protein atoms were harmonically restrained. The systems were equilibrated in the NPT ensemble for 500 ps at 300K, after which the protein RMSD and total energy remained constant.

All simulations were performed using cubic periodic boundary conditions. Long-range electrostatic interactions were calculated using the particle mesh Ewald method [22, 23] with a short range cuto of 9 Å. Van der Waals interactions were computed using a cuto of 14 Å. For NPT equilbration, the temperature and pressure were controlled via weak coupling to an external bath [24] with a temperature coupling time constant of 1 ps, pressure coupling time constant of 0.5 ps and isothermal compressibility of 4.5×10^{-5} bar^{-1}. The temperature of the NVT simulations was controlled using a Nose-Hoover thermostat [25, 26] with a 0.1 ps damping coefficient. The LINCS [18] and SETTLE algorithms [27] were used to constrain bond lengths, which permitted a 2 fs timestep.

2.2. Electronic Structure Calculations

Electronic structure calculations (section 4) were performed using the Gaussian09 software package [28]. We used the PBE0 functional [29, 30, 31, 32] and the 6-311++G** basis set using a polarizable continuum model with conductor like solvations [33, 34] to simulate the active site within an aqueous environment.

3. IR Spectra

The IR spectra of PYP were simulated using an effective vibrational Hamiltonian which can be recast using the bosonic creation ($b_i^\dagger$) and annihilation (b_i) operators [35, 36, 37]:

$$H(t)=\hbar\sum_i \omega_i(t)\, b_i^\dagger b_i+\hbar\sum_{i,j} J_{ij}(t)\, b_i^\dagger b_j+\frac{\hbar}{2}\sum_i \Delta_i b_i^\dagger b_i^\dagger b_i b_i \quad (1)$$

ω_i and Δ_i are the fundamental frequency and the anharmonicity of mode i respectively, and J_{ij} is the coupling between modes i and j. The interaction of the vibrational system with the field is given by:

$$H'(t)=\sum_i \mu_i(t)\cdot \boldsymbol{E}(t)\left(b_i+b_i^\dagger\right) \quad (2)$$

In the Hamiltonian, we include 126 modes in the carbonyl stretching region: 124 amide I modes, the Glu46 COOH side chain stretching mode, and the pCA C=O stretch. We have used electrostatic DFT maps from the literature to evaluate the fluctuating parameters in $H(t)$ and $H'(t)$ for the amide I and COOH vibrations. For the amide I vibrations, the electrostatic DFT map of [38] was used to evaluate $\omega(t)$ while the transition dipole was fixed to the gas phase value [39] and the anharmonicity was fixed to the measured value of -16 cm^{-1}[40]. The Glu46 carboxylic acid vibration was modeled using the electrostatic DFT map in reference [41]. We have further constructed a new electrostatic DFT map for the pCA C=O stretch. Details are given in the supporting information. J_{ij} was given by the transition-dipole coupling model. The nearest-neighbor coupling between amide I modes was given by the Torii and Tatsumi dihedral angles map [42].

3.1. IR Absorption

All simulations were performed in the inhomogeneous limit by averaging over 2000 configurations taken from 4 ns MD simulations. The field-free frequencies of the amide-I modes and the Glu46 COOH mode were set to 1681 $cm^{-1}$and 1745 cm^{-1}respectively to match experimental results [43]. Likewise, a shift of -75 $cm^{-1}$was applied to the cis and trans pCA C=O stretching modes to match experimental results [17]. Note that the same shift was applied to each isomer. The homogeneous vibrational dephasing was fixed to 5.5 $cm^{-1}$for all transitions.

The simulated spectrum of pG is shown in figure 2. It compares well with experiment. The spectrum is dominated by the amide I band, centered around 1640 $cm^{-1}$with a full-width half-maximum of 40.6 cm^{-1}. The band below 1600 cm^{-1}in the experimental spectrum is due to absorption of the amide II and carboxylate modes which are not included in the simulations.

The calculated difference absorption spectrum between the pG and pR states is presented in figure 3. It shows two positive-negative features corresponding to changes in the amide I and Glu46 COOH bands. The dominant feature is caused by the amide I modes while the smaller signal is caused by the Glu46 COOH mode. Minima in the difference spectrum are assigned to pG and maxima are assigned to pR.

The amide I band shifts from 1665 cm^{-1}in pG (peak I' in figure 3) to 1633 cm^{-1}(peak I in figure 3) in pR resulting in the amide I shift of 1633-1665=−32 cm^{-1}. Likewise, the Glu46 COOH shifts from 1742 cm^{-1}in pG (peak II' in figure 3) to 1723 cm^{-1}(peak II in figure 3) in pR resulting in the Glu46 COOH shift of 1723-1742=−19 cm^{-1}. The simulated amide I shift of −32 cm^{-1}compares to the experimental value of −17 cm^{-1}[14, 16] while the simulated Glu46 COOH shift of −17 cm^{-1}compares to the experimental value of −8 cm^{-1}[13, 14, 16]. The simulations overestimate the magnitude of the amide I and Glu46 COOH shifts, however the sign of the shifts are correct. This demonstrates that MD simulations in combination with electrostatic DFT maps can qualitatively predict frequency shifts in the carbonyl stretching region. The shift of the pCA C=O stretch cannot be accurately determined from the difference IR absorption due to its overlap with the amide I band. This may be due to the relatively weak oscillator strength of the pCA C=O stretch. Inclusion of anharmonic coupling of the C=O stretch to other vibrational modes of the chromophore in the electrostatic DFT map could potentially increase its oscillator strength (see Supporting Information). The shift of the pCA C=O stretch is easily determined from RR spectra where only the chromophore vibrational modes are observed [17]. This shift has also been observed in excited state IR difference spectra of PYP mutants [44]. In that experiment, the protein backbone does not have time to react to the chromophore isomerization due to the short delay between the visible pump and IR probe and the pCA C=O stretch can be clearly observed.

It has been determined in the literature that the shift in the Glu46 COOH band is caused by a change in the distance of Glu46 and pCA [13, 14]. Contributions from nearby bands that are not included in our simulations may make this measurement more complicated in experiments. In pR, Glu46 moves slightly closer to the phenolate anion of pCA to precipitate the proton transfer from Glu46 to pCA. This movement causes a slight red-shift in the Glu46 COOH stretching band [13, 14, 16]. The difference spectrum in the region of the Glu46 COOH stretch was fit to a sum of two Gaussians:

$$\Delta I(\omega) = \sum_{i=1}^{2} A_i \exp\left[-\frac{(\omega-\omega_i)^2}{2\sigma_i^2}\right] \quad (3)$$

The results of the fit are presented in table 1.

The central frequency of the pG and pR Glu46 COOH stretch is correlated with the average distance between the Glu46 hydrogen atom and the anionic oxygen of pCA. In pR, where Glu46 and pCA have an average distance of less than 2 Å, the central frequency is lower than in pG where the average distance is greater than 3 Å. Our findings confirm the experimental findings of references [13, 14, 16]. It should be noted that IR difference spectra at short delay times (up to ≈800 ps), do not show a frequency red-shift of the Glu46 COOD

band following the decay of the excited state. This was first attributed by Groot *et al.* [45] to an unrelaxed pR state and was later confirmed by Heyne *et al.* [46].

The linewidths of the Glu46 COOH stretching peaks can similarly be related to the fluctuations in the active site of the protein. In the pG MD simulation, the distance between Glu46 and pCA fluctuates more than in the pR simulation and therefore, this leads to a larger FWHM due to a larger degree of inhomogeneous broadening. The larger structural fluctuations in pG are caused by Glu46 being occasionally forced out of the hydrogen bonding position with pCA. The hydrogen bond is typically replaced by the side chain of Thr50 while Glu46 then forms a hydrogen bond with the amide backbone of Thr50. This conformational mobility of Glu46 in pG has been observed in room temperature liquid state NMR studies [47].

Experimental IR difference spectra of PYP have observed the frequency shift of the Glu46 COOH stretch, however, the differences in the linewidths of the Glu46 COOH peak have not been observed. In the steady-state experiments of Ho et al. [13], the Glu46 COOH difference band was observed to have similar linewidths for pG and pR. This is likely due to the low temperatures (80K) that were used during these experiments. In room temperature species associated difference spectroscopy experiments [45], the linewidths of the Glu46 COOH peak cannot be accurately assessed due to the small number of data points used for fitting in this region.

3.2. 2D-IR

The 2D-IR spectra were calculated in the rephasing direction ($k_I = -k_1 + k_2 + k_3$) with all pulses colinear and with the same polarization (*xxxx*). The spectra were calculated using the quasiparticle approach based on the nonlinear exciton equations [48, 49, 50, 35] as implemented in SPECTRON [36]. The real-space excitonic overlap [49] was truncated at a value of 0.5 and t_2 was set to 0 fs. All spectra were normalized to a maximum absolute value of 1.0.

The 2D-IR spectra of pG and pR are shown in figure 4. The region plotted only includes the amide I and pCA C=O stretch. The simulated 2D-IR spectra of pG and pR are nearly identical with a single inhomogeneously broadened peak near $\omega_1 = \omega = 1640\ cm^{-1}$ that is dominated by the amide I modes. The difference 2DIR spectrum (pR-pG) shown in figure 4c reveals the red-shift of the amide I band in pR compared to pG. While the pCA C=O stretch is also included in this band, it cannot be effectively deconvoluted from the amide I modes.

The linear absorption spectra can already distinguish between the pG and pR states and the 2DIR does not provide much new information. However, by isotope-labeling certain secondary strutcural elements (e.g. specific α-helices and β strands), it may be possible to gain new information from 2DIR spectra. We further note that the coupling to other modes (e.g. C=C stretches) are not observed in the simulated 2DIR spectra as they are not explicitly included in the Hamiltonian. The coupling of C=O stretching modes with other types of modes could provide additional spectroscopic signatures.

4. Resonance Raman Spectroscopy

In RR spectroscopy, we only consider vibrations which are coupled to a given electronic transition. The electronic Hamiltonian is given by:

$$H = |g\rangle H_g \langle g| + |e\rangle H_e \langle e| \quad (4)$$

where H_g is the ground state vibrational Hamiltonian and H_e is the excited state vibrational Hamiltonian. To describe the ground state and excited state vibrational Hamiltonians, we will assume that the vibrations are modeled as linearly displaced harmonic oscillators. The ground state and excited state vibrational Hamiltonians are:

$$H_g = H_{B,g} + \frac{\hbar}{2}\sum_i^N \omega_i \left(p_i^2 + q_i^2\right) \quad (5a)$$

$$H_e = \hbar\omega_{eg}^0 + H_{B,e} + \frac{\hbar}{2}\sum_i^N \omega_i \left(p_i^2 + (q_i + \delta_i)^2\right) \quad (5b)$$

where ω_i is the frequency of the i-th normal mode, q_i and p_i are the dimensionless coordinates for vibration i, and δ_i is the dimensionless displacement of vibration i. $H_{B,g}$ and $H_{B,e}$ are the bath Hamiltonians.

To make a connection with equation 1, we can rewrite equation 6 using the creation and annihilation operators:

$$H = |g\rangle H_g \langle g| + |e\rangle H_e \langle e| \quad (6a)$$

$$H_g = H_{B,g} + \hbar\sum_i^N \omega_i b_i^\dagger b_i \quad (6b)$$

$$H_e = \hbar\omega_{eg}^0 + H_{B,e} + \hbar\left[\sum_i^N \omega_i b_i^\dagger b_i + \frac{1}{\sqrt{2}}\left(b_i^\dagger + b_i\right) + \frac{\delta_i^2}{2}\right] \quad (6c)$$

It should also be noted that the ground state Hamiltonian of equation 1 collapses into H_g when $J_{ij} = 0$ and $\Delta_I = 0$.

For all further calculations, we will use an extended description of the chromophore which includes the active site residues Glu46, Tyr42, and Cys69 (figure 5). We refer to these structures as the active site fragments of pG and pR. Glu46 is represented by CH_3O_2H and Tyr42 is represented by CH_3OH. In the pG state, Cys69 is represented by H_2O. We do not include Cys69 in the pR state as it does not make a hydrogen bond with the chromphore. The sulfur atom of the chromophore is capped with a methyl group in pG and pR. In the Hamiltonian (equation 6), we include all modes between 400 $cm^{-1}$and 2000 cm^{-1}(63 modes for pG and 64 modes for pR). We note that the model used for the RR simulations differs from the IR simulations. The RR simulations include only chromophore modes in the range 400-2000 cm^{-1}while the IR simulations consider all C=O stretching modes in the protein. We only consider the low-lying $\pi - \pi^*$ transition, which is calculated as 24356 $cm^{-1}$for pG and 25082 $cm^{-1}$for pR. In our calculations, the nearest excited states occur at 34115 $cm^{-1}$for pG and 31937 $cm^{-1}$for pR. The $\pi - \pi^*$ transition has previously been shown to be isolated from all other transitions [51, 52]. The displacements, δ_i, are calculated using the gradients of the ground and excited state potential energy surfaces [53, 54, 55]:

$$\delta_i = \frac{1}{\hbar\omega_i}\frac{\partial\left(E_e - E_g\right)}{\partial_{q_i}} \quad (7)$$

4.1. Electronic Absorption

To calculate the visible linear absorption spectrum, we will use the cumulant expansion technique [56]. The linear absorption spectrum is given by:

$$\sigma(\omega) = -\frac{i}{\hbar}\mu_{ge}\mu_{eg}\int_0^\infty dt e^{i\omega t}e^{-i\omega_{eg}t-\gamma_{eg}t-g(t)} \quad (8)$$

where ω_{eg} is the transition frequency from the ground to excited electronic state, μ_{ij} is the transition dipole from states j and i, and γ_{eg} is the homogeneous electronic dephasing. The line broadening function $g(t)$ will include the effects of coupling between the electronic transition and intramolecular vibrations as well as the electronic transition and the fluctuations of the protein and solvent.

We have used the Brownian oscillator model to model the coupling of the electronic transition to the fluctuating protein and solvent [56]. The frequency-frequency correlation function was fit to [56]:

$$\langle \delta\omega_{eg}(t)\,\delta\omega_{eg}(0)\rangle = \Delta^2 e^{-\Lambda t} \quad (9)$$

where Δ is the amplitude of the fluctuations and Λ^{-1} is their correlation time. The dimensionless parameter, $k = \Lambda/\Delta$ was evaluated to determine the timescale of the bath. From a 2 ps MD simulation of the solvated protein, snapshots were saved every 8 fs. For each snapshot, the active site fragment was replaced by the PBE0/6-311++G** optimized structure and all surrounding atoms within 20 Åof the active site were replaced by their MM point charges to generate a background charge density. TDDFT calculations were then performed to calculate the low-lying π-π* excitation energy for each snapshot and the frequency-frequency correlation function was calculated 6. The results of the fit are presented in table 2. For both pG and pR, the interaction with the bath is strongly inhomogeneous. The magnitude of the fluctuations induced by the bath agree with a previous QM/MM study [52].

Including the coupling of the electronic system to the intramolecular vibrations and the strongly inhomogeneous bath results in a line-broadening function $g(t)$:

$$g(t) = \frac{\Delta^2}{2}t^2 + \sum_j \frac{\delta_j^2}{2}\left[\left(\coth\left(\beta\hbar\omega_j/2\right)\right)\left(1-\cos\left(\omega_j t\right)\right) + i\left(\sin\left(\omega_j t\right)-\omega_j t\right)\right] \quad (10)$$

The simulated visible absorption spectra of pG and pR are shown in figure 7. The simualted spectra have an overall blue shift when compared to experiment as has been observed in previous computational studies [51, 57, 58, 52, 59, 60]. The simulated pR spectrum is blue-shifted from the simulated pG spectrum, which is contrary to the experimental result. Inclusion of a larger number of residues can give more accurate excitation energies [20], however, the computational cost increases greatly. However, the directionality of the frequency shift only changes the relative resonance enhancement of the Raman transitions between the two intermediates. As we will demonstrate in the following section, we believe we have calculated the correct excited state transition for pG and pR based on comparison with the experimental spontaneous-RR spectra.

4.2. Spontaneous Resonance Raman Spectroscopy

The spontaneous RR spectra were calculated using the effective polarizability given in equation A12 of reference [62]. We assume the impulsive limit and the lineshape function,

$g_e^{j'}(t)$ includes an additional additive contribution from the fluctuating protein-solvent as in equation 10. The spectra were calculated using an incident frequency (ω_j) which was set to the frequency of maximum absorption of pG (24390 cm^{-1}). We set the homogeneous electronic dephasing γ_{eg} to 100 cm^{-1}. The simulated spectra for are compared to experiment [17] in figure 8 and mode assignments are given in tables S3 and S4. Our simulations reveal that the C=O stretching mode, shaded in pink in figure 8, shifts from 1689 cm^{-1}in pG to 1714 cm^{-1}in pR due to the breakage of the hydrogen bond to the Cys69 backbone. This peak is also significantly more intense in pR than in pG. This change in intensity is caused by the difference of the value of the displacements for the C=O stretch, $\delta_{C=O}$, relative to the displacements for the strongest C=C+C=C(ph) stretch, $\delta_{C=C}$. The strongest C=C+C=C(ph) stretch at 1593 $cm^{-1}$is dominated by the vinyllic C=C rather than aromatic C=C stretch. In pG, the $\delta_{C=O}/\delta_{C=C}$ = 0.11/0.50 = 0.22 and in pR, $\delta_{C=O}/\delta_{C=C}$ = 0.30/0.35 = 0.86. In the experiment, the C=O stretching mode is nearly silent at 1633 cm^{-1}in pG, however, upon formation of pR, this mode shifts to 1666 $cm^{-1}$and shows a significant increase in intensity [17].

4.3. One-dimensional stimulated Resonance Raman Spectra (1D-SRR)

The one-dimensional stimulated resonance Raman (1D-SRR) spectra were calculated using an effective polarizability which is given by equations (A11) and (A14) of reference [62].

The lineshape function, $g_e^{j'}(t)$ includes an additional additive contribution from the fluctuating protein-solvent as in equation 10. We calculate the spectra using a 5 fs pump pulse centered at 22141 $cm^{-1}$and a 5 fs probe pulse was set to the frequency of maximum absorption (24390 $cm^{-1}$for pG, 25126 $cm^{-1}$for pR). The resonance offset is intended to ensure that the excited-state contribution to the signal is small compared to the ground state contribution. We define the parameter:

$$\zeta = \frac{\left\langle \psi_e^{(1)} | \psi_e^{(1)} \right\rangle}{\sqrt{\left\langle \psi_g^{(2)} | \psi_g^{(2)} \right\rangle}} \quad (11)$$

where $\left|\psi_e^{(1)}\right\rangle$ and $\left|\psi_g^{(2)}\right\rangle$ are the nuclear wavefunctions on the ground and electronic states which are first and second order in the field respectively. The detunings used here were chosen such that $\zeta \leq 0.1$. The simulations included a vibrational dephasing of 10 cm^{-1}. The 1D-SRR spectra are shown in figure 9. By comparing the spontaneous RR spectra (figure 8) with the 1D-SRR spectra, it is seen that the 1D-SRR spectra are similar to the spontaneous RR spectra. Both the spontaneous RR and 1D-SRR spectra reveal that the chromophore C=O stretching mode occurs at higher frequency with a higher intensity in pR.

4.4. Two-dimensional stimulated Resonance Raman (2D-SRR) Spectra

The two-dimensional stimulated resonance Raman (2D-SRR) signals are given by the four loop diagrams in figure 10. The 2D-SRR spectra were calculated using equation (A11) of reference [62] with an effective polarizability given by equations (A14-A22). The lineshape function, $g_e^{j'}(t)$ includes an additional additive contribution from the fluctuating protein-solvent as in equation 10. fs pulses centered at 22141 $cm^{-1}$for the pump pulses, k_1 and k_2. The probe pulse, k_3 was a 5 fs pulse centered around the frequency of maximum absorption (24390 $cm^{-1}$for pG, 25126 $cm^{-1}$for pR). As in the 1D-SRR simulations, the pump pulses are pre-resonant to ensure that the excited-state contribution is small compared to the ground state contribution. We have used a homogeneous vibrational dephasing of 10 cm^{-1}.

The absolute value of the 2D-SRR spectra for pG and pR are shown in 11. Spectra were plotted on a non-linear scale arcsinh (cS) where S represents the signal, normalized to a maximum absolute value of 1, and c is a scaling factor which is set to 10. The most dramatic change between the 2D-SRR spectra of pG and pR are the cross peaks associated with the C=O stretch that are absent in pG but present in pR. In pG, these cross peaks, which are extremely weak, are along the horizontal slice ω_2 = 1689 cm^{-1}and along the semi-diagonal slice $\omega_2 = \omega_1 - 1689$ cm^{-}. In pR, these cross peaks appear along the horizontal slice ω_2 = 1714 cm^{-1}and along the semi-diagonal slice $\omega_2 = \omega_1 - 1714$ cm^{-}. The appearance of these cross peaks in the pR spectrum provides an additional feature to distinguish between pG and pR.

In figure 12, we present the 2D-SRR spectra in the the region ($1500 < \omega_1 < 1800$, 1500, $\omega_2 <$ 1800)to emphasize the difference in the cross peaks associated with the C=O stretch in the pG and pR 2D-SRR spectra. This region of the spectrum only includes contributions from C=O and C=C stretching modes. In the pG spectrum, there are two diagonal transitions which result from the C=C+C=C(ph) stretching mode at (1593 cm^{-1},1593 cm^{-1}) and the C=C+C=C (ph) stretching mode at (1539 cm^{-1},1539 cm^{-1}). There are also cross peaks which appear at (1539 cm^{-1},1593 cm^{-1}) and (1593 cm^{-1},1539 cm^{-1}). In the pR spectrum, all four of these peaks are present, but there are five new peaks which are associated with the C=O stretch. The diagonal C=O stretching peak at (1714 cm^{-1}, 1714 cm^{-1}) appears and there are cross peaks between the C=O stretch and the C=C+C=C(ph) stretch at 1593 cm^{-1}located at (1714 cm^{-1}, 1593 cm^{-1}) and (1593 cm^{-1}, 1714 cm^{-1}). Cross peaks between the C=O stretch and the C=C+C=C(ph) at 1537 cm^{-1}stretch occur at (1714 cm^{-1}, 1537 cm^{-1}) and (1537 cm^{-1}, 1714 cm^{-1}). The difference spectrum (pR-pG) (panel c of figure 12) reveals clear signatures of the new off-diagonal peaks that appear in pR, which can be seen at (1714 cm^{-1}, 1593 cm^{-1}), (1593 cm^{-1}, 1714 cm^{-1}), (1714 cm^{-1}, 1537 cm^{-1}), and (1537 cm^{-1}, 1714 cm^{-1}).

The cross peaks between the C=O and C=C+C=C(ph) stretching modes in figure 12 arise from diagram (iv) in figure 10 when $g' \neq g''$. According to these diagrams, the peak intensities are proportional to $\alpha^{(3)}_{gg''}\alpha^{(2)}_{g''g'}\alpha^{(1)}_{g'g}$. Therefore, these cross peaks contain 'intermode' elements of the polarizability, $\alpha_{g''g'}$, which may not be probed by spontaneous or 1D-SRR spectroscopy. These elements are inherently related to the chromophore structure and dynamics as projected onto the vibrational modes g' and g''.

The diagonal ($\omega_1 = \omega_2$) slices of the 2D-SRR spectra are shown in figure 13. As in the spontaneous and 1D-SRR spectra, the C=O stretching diagonal peak is much more intense in pR and occurs at a higher frequency compared to pG.

The slices of the 2D-SRR spectra along ω_2 = 1689 cm^{-1}for pG and ω_2 = 1714 cm^{-1}for pR are plotted in panels B_{pG} and B_{pR} of figure 14. The horizontal slice is more intense in pR compared to pG. Additionally, in the pR spectrum, the diagonal C=O stretch, which appears at 1681 cm^{-1}for pG and 1714 cm^{-1}for pR, has a much higher relative intensity compared to the cross peak of the C=O stretch with the C=C+C=C(ph) stretching mode, which appears at 1593 cm^{-1}in pG and pR. In fact, the slice along ω_2 = 1689 cm^{-1}for pG is dominated by this cross peak.

The slices of the 2D-SRR spectra along the semi-diagonal that are associated with the C=O stretch ($\omega_2 = \omega_1 - 1689$ cm^{-1}for pG and $\omega_2 = \omega_1 - 1714$ cm^{-1}for pR) are shown in panels C_{pG} and C_{pR} of figure 14 for pG and pR respectively. Due to the Lorentzian lineshapes in the current calculations, there are peaks which appear in these slices due to the tails of nearby peaks in the ω_1 direction. We have plotted the stick spectrum with the slices to ensure that no false peaks were analyzed. The intensity of this slice in pG is much weaker

than in pR. This is similar to the horizontal slices in B_{pG} and B_{pR} where the cross peaks associated with the C=O stretch in pG were much weaker compared to the cross peaks associated with the C=O stretch in pR.

If C=C modes were to be included in the IR simulations (equation 1), the C=C stretching/ C=O stretching cross peaks in the 2DIR spectra would probe the coupling of C=C and C=O stretches in the protein. However, due to the high degree of degeneracy of C=O and C=C transitions, only the average coupling of these bands would be observed unless specific modes could be spectrally isolated (e.g. by site-specific isotope labeling). RR spectroscopy only probes vibrational modes coupled to the chromophore excited state transition. We can then clearly assign the cross peaks in the 2D-SRR spectra to two different vibrational modes of the chromophore. This provides a clear view of local structure variations of the chromophore.

5. Conclusions

Simulations of IR and RR spectra of the pG and pR intermediates of PYP provide complementary information in photosensors. The difference linear IR absorption spectrum (pR-pG) reveals an amide I shift and a shift of the Glu46 COOH mode, both of which have been experimentally observed. A careful analysis of the Glu46 COOH difference band revealed that the pR state has a narrower linewidth than the pG state which is caused by the fact that the Glu46(H)-pCA(O-) hydrogen bond is held more tightly in the pR state. The rephasing 2D-IR using the *xxxx* polarization were also calculated and revealed the shift in the amide I band.

The simulated sponatneous RR spectra agree well with experiment. The spontaneous RR spectra reveal a blue-shift and an increase in intensity of the C=O stretching peak. The simulated 1D-SRR spectra of pG and pR are similar to the sponanteous RR spectra and also reveal the blue-shift and increase in intensity of the C=O stretch. The 2D-SRR spectrum of pR has cross peaks associated with the C=O stretch that do not appear in pG. Due to the novel information contained in the 2D-SRR spectra, we see this as a new method of probing chromophores in hosts, particularly in photosensors.

Supplementary Material

Refer to Web version on PubMed Central for supplementary material.

Acknowledgments

The authors gratefully acknowledge Dr. Jocelyne Vreede (Vrije Universiteit Amsterdam) for providing the force eld for pCA. The research leading to these results has received funding from the National Institutes of Health (grants GM059230 and GM091364) and the National Science Foundation (grant CHE-1058791). N.K.P. is supported by a National Science Foundation Graduate Research Fellowship.

References

[1]. Dugave, C., editor. Cis-trans Isomerization in Biochemistry. Wiley-VCH; Weinheim: 2006.

[2]. Larsen, DS.; van Grondelle, R.; Hellingwerf, KJ. Primary Photochemistry in the Photoactive Yellow Protein: The Prototype Xanthopsin. In: Braun, M.; Gilch, P.; Zinth, W., editors. Ultrashort Laser Pulses in Biology and Medicine. Springer; New York: 2008. p. 165-199.

[3]. Hellingwerf KJ, Hendriks J, Gensch T. Photoactive Yellow Protein, A New Type of Photoreceptor Protein: Will This Yellow Lab? Bring Us Where We Want to Go? J. Phys. Chem. A. 2003; 107:1082–1094.

[4]. Groot ML, van Wilderen LJGW, Di Donato M. Time-resolved methods in biophysics. 5. Femtosecond time-resolved and dispersed infrared spectroscopy on proteins. Photochem. Photobiol. Sci. 2007; 6:501–7. [PubMed: 17487299]

[5]. Borgstahl GEO, Williams DR, Getzoff ED. 1.4 ÅStructure of Photoactive Yellow Protein, a Cytosolic Photoreceptor: Unusual Fold. Active Site, and Chromophore, Biochem. 1995; 34:6278–6287.

[6]. Hoff WD, van Stokkum IHM, van Ramesdonk HJ, van Brederode ME, Brouwer AM, Fitch JC, Meyer TE, van Grondelle R, Hellingwerf KJ. Measurement and global analysis of the absorbance changes in the photocycle of the photoactive yellow protein from Ectothiorhodospira halophila. Biophys. J. 1994; 67:1691–705. [PubMed: 7819501]

[7]. Genick UK, Borgstahl GEO, Ng K, Ren Z, Pradervand C, Burke PM, rajer V, Teng T-Y, Schildkamp W, McRee DE, Moffat K, Getzoff ED. Structure of a protein photocycle intermediate by millisecond time-resolved crystallography. Science. 1997; 275:1471–1475. [PubMed: 9045611]

[8]. Genick UK, Soltis SM, Kuhn P, Canestrelli IL, Getzoff ED. Structure at 0.85 Åresolution of an early protein photocycle intermediate. Nature. 1998; 392:206–9. [PubMed: 9515969]

[9]. Getzoff ED, Gutwin KN, Genick UK. Anticipatory active-site motions and chromophore distortion prime photoreceptor PYP for light activation. Nat. Struct. Biol. 2003; 10:663–8. [PubMed: 12872160]

[10]. Anderson S, Crosson S, Moffat K. Short hydrogen bonds in photoactive yellow protein. Acta Crystallogr., Sect. D, Biol. Crystallogr. 2004; 60:1008–16. [PubMed: 15159559]

[11]. Ihee H, Rajagopal S, Srajer V, Pahl R, Anderson S, Schmidt M, Schotte F, Anfinrud P. a. Wul M, Moffat K. Visualizing reaction pathways in photoactive yellow protein from nanoseconds to seconds. Proc. Natl. Acad. Sci. U. S. A. 2005; 102:7145–50. [PubMed: 15870207]

[12]. Kim SK, Pedersen S, Zewail AH. Femtochemistry of organometallics: dynamics of metal-metal and metal-ligand bond cleavage in M2(CO)10. Chem. Phys. Lett. 1995; 233:500–508.

[13]. Xie A, Hoff WD, Kroon AR, Hellingwerf KJ. Accelerated Publications Glu46 Donates a Proton to the 4-Hydroxycinnamate Anion Chromophore During the Photocycle of Photoactive Yellow Protein. Biochem. 1996; 35:14671–14678. [PubMed: 8942626]

[14]. Imamoto Y, Mihara K, Hisatomi O, Kataoka M, Tokunaga F, Bojkova N, Yoshihara K. Evidence for proton transfer from Glu-46 to the chromophore during the photocycle of photoactive yellow protein. J. Biol. Chem. 1997; 272:12905–8. [PubMed: 9148894]

[15]. Hoff WD, Xie A, Van Stokkum IH, Tang XJ, Gural J, Kroon R, Hellingwerf KJ. Global conformational changes upon receptor stimulation in photoactive yellow protein. Biochem. 1999; 38:1009–17. [PubMed: 9893997]

[16]. Brudler R, Rammelsberg R, Woo TT, Getzoff ED, Gerwert K. Structure of the I1 early intermediate of photoactive yellow protein by FTIR spectroscopy. Nat. Struct. Bio. 2001; 8:265–70. [PubMed: 11224574]

[17]. Pan DH, Philip A, Hoff WD, Mathies RA. Time-resolved resonance Raman structural studies of the pB' intermediate in the photocycle of photoactive yellow protein. Biophys. J. 2004; 86:2374–2382. [PubMed: 15041675]

[18]. Hess B. P-LINCS: A Parallel Linear Constraint Solver for Molecular Simulation. J. Chem. Theory Comput. 2008; 4:116–122.

[19]. Daura X, Mark AE, Van Gunsteren WF. Parametrization of aliphatic CHn united atoms of GROMOS96 force field. J. Comput. Chem. 1998; 19:535–547.

[20]. Groenhof G, Lensink MF, Berendsen HJC, Mark AE. Signal transduction in the photoactive yellow protein. II. Proton transfer initiates conformational changes. Proteins. 2002; 48:212–9. [PubMed: 12112690]

[21]. Berendsen, HJ.; Postma, JPM.; Van Gunsteren, WF.; Hermans, J. Interaction models for water in relation to protein hydration. In: Pullman, B., editor. Intermolecular Forces. Reidel; Dordrecht: 1981. p. 331-342.

[22]. Darden T, York D, Pedersen L. Particle mesh Ewald: An N log(N) method for Ewald sums in large systems. J. Chem. Phys. 1993; 98:10089–10092.

[23]. Essmann U, Perera L, Berkowitz ML, Darden T, Lee H, Pedersen L. A smooth particle mesh Ewald method. J. Chem. Phys. 1995; 103:8577–8593.

[24]. Berendsen HJC, Postma JPM, van Gunsteren WF, DiNola A, Haak JR. Molecular dynamics with coupling to an external bath. J. Chem. Phys. 1984; 81:3684.

[25]. Hoover WG. Canonical dynamics: Equilibrium phase-space distributions. Phys. Rev. A. 1985; 31:1695–1697. [PubMed: 9895674]

[26]. Nosé S. An extension of the canonical ensemble molecular dynamics method. Mol. Phys. 1986; 57:187–191.

[27]. Miyamoto S, Kollman PA. Settle: An analytical version of the SHAKE and RATTLE algorithm for rigid water models. J. Comput. Chem. 1992; 13:952–962.

[28]. Frisch, MJ.; Trucks, GW.; Schlegel, HB., et al. Gaussian 09, Revision A.1. Gaussian, Inc.; Wallingford CT: 2009.

[29]. Perdew J, Burke K, Ernzerhof M. Generalized Gradient Approximation Made Simple. Phys. Rev. Lett. 1996; 77:3865–3868. [PubMed: 10062328]

[30]. Perdew JP, Burke K, Ernzerhof M. Generalized Gradient Approximation Made Simple [Phys. Rev. Lett. 77, 3865 (1996)]. Phys. Rev. Lett. 1997; 78:1396–1396.

[31]. Adamo C. Toward reliable density functional methods without adjustable parameters: The PBE0 model. J. Chem. Phys. 1999; 110:6158–6170.

[32]. Amos RD. Electric and magnetic properties of CO, HF, HCI, and CH3F. Chem. Phys. Lett. 1982; 87:23–26.

[33]. Barone V, Cossi M. Quantum Calculation of Molecular Energies and Energy Gradients in Solution by a Conductor Solvent Model. J. Phys. Chem. A. 1998; 102:1995–2001.

[34]. Cossi M, Rega N, Scalmani G, Barone V. Energies, structures, and electronic properties of molecules in solution with the C-PCM solvation model. J. Comput. Chem. 2003; 24:669–81. [PubMed: 12666158]

[35]. Mukamel S. Multidimensional Femtosecond Correlation Spectroscopies of Electronic and Vibrational Excitations. Annu. Rev. Phys. Chem. 2000; 51:691–729. [PubMed: 11031297]

[36]. Zhuang W, Abramavicius D, Hayashi T, Mukamel S. Simulation protocols for coherent femtosecond vibrational spectra of peptides. J. Phys. Chem. B. 2006; 110:3362–74. [PubMed: 16494351]

[37]. Zhuang W, Hayashi T, Mukamel S. Coherent multidimensional vibrational spectroscopy of biomolecules: concepts, simulations, and challenges. Angew. Chem., Int. Ed. 2009; 48:3750–81.

[38]. Hayashi T, Zhuang W, Mukamel S. Electrostatic DFT Map for the Complete Vibrational Amide Band of NMA. J. Phys. Chem. A. 2005; 109:9747–9759. [PubMed: 16833288]

[39]. Kubelka J, Keiderling TA. Ab Initio Calculation of Amide Carbonyl Stretch Vibrational Frequencies in Solution with Modified Basis Sets. 1. N-Methyl Acetamide. J. Phys. Chem. A. 2001; 105:10922–10928.

[40]. Hamm P, Lim M, Hochstrasser RM. Structure of the amide i band of peptides measured by femtosecond nonlinear-infrared spectroscopy. J. Phys. Chem. B. 1998; 102:6123–6138.

[41]. Bagchi S, Falvo C, Mukamel S, Hochstrasser RM. 2D-IR experiments and simulations of the coupling between amide-I and ionizable side chains in proteins: application to the Villin headpiece. J. Phys. Chem. B. 2009; 113:11260–73. [PubMed: 19618902]

[42]. Torii H, Tasumi M. Model calculations on the amide-I infrared bands of globular proteins. J. Chem. Phys. 1992; 96:3379.

[43]. Xie A, Kelemen L, Redlich B, Vandermeer L, Austin R. Picosecond visible/IR pumpprobe dynamics of photoactive yellow protein. Nucl. Instrum. Methods Phys. Res., Sect. A. 2004; 528:605–608.

[44]. Rupenyan AB, Vreede J, van Stokkum IHM, Hospes M, Kennis JTM, Hellingwerf KJ, Groot ML. Proline 68 enhances photoisomerization yield in photoactive yellow protein. J. Phys. Chem. B. 2011; 115:6668–6677. [PubMed: 21542640]

[45]. Groot ML, Wilderen LJGWV, Larsen DS, Horst MAVD, Stokkum IHMV, Hellingwerf KJ, Grondelle RV. Initial Steps of Signal Generation in Photoactive Yellow Protein Revealed with

Femtosecond Mid-Infrared Spectroscopy. Biochem. 2003; 42:10054–10059. [PubMed: 12939133]

[46]. Heyne K, Mohammed OF, Usman A, Dreyer J, Nibbering ETJ, Cusanovich MA. Structural evolution of the chromophore in the primary stages of trans/cis isomerization in photoactive yellow protein. J. Am. Chem. Soc. 2005; 127:18100–6. [PubMed: 16366562]

[47]. Dux P, Rubinstenn G, Vuister GW, Boelens R, Mulder FAA, Hard K, Hoff WD, Kroon AR, Crielaard W, Hellingwerf KJ, Kaptein R. Solution structure and backbone dynamics of the photoactive yellow protein. Biochem. 1998; 37:12689–99. [PubMed: 9737845]

[48]. Abramavicius D, Palmieri B, Voronine DV, Sanda F, Mukamel S. Coherent multidimensional optical spectroscopy of excitons in molecular aggregates; quasiparticle versus supermolecule perspectives. Chem. Rev. 2009; 109:2350–408. [PubMed: 19432416]

[49]. Chernyak V, Zhang WM, Mukamel S. Multidimensional femtosecond spectroscopies of molecular aggregates and semiconductor nanostructures: The nonlinear exciton equations. J. Chem. Phys. 1998; 109:9587–9601.

[50]. Zhang WM, Chernyak V, Mukamel S. Multidimensional femtosecond correlation spectroscopies of electronic and vibrational excitons. J. Chem. Phys. 1999; 110:5011–5028.

[51]. Molina V, Merchán M. On the absorbance changes in the photocycle of the photoactive yellow protein: a quantum-chemical analysis. Proc. Natl. Acad. Sci. U. S. A. 2001; 98:4299–304. [PubMed: 11287643]

[52]. Gromov EV, Burghardt I, Köppel H, Cederbaum LS. Electronic structure of the PYP chromophore in its native protein environment. J. Am. Chem. Soc. 2007; 129:6798–806. [PubMed: 17474743]

[53]. Ren H, Jiang J, Mukamel S. Deep UV resonance Raman spectroscopy of β-sheet amyloid fibrils: a QM/MM simulation. J. Phys. Chem. B. 2011; 115:13955–62. [PubMed: 22007849]

[54]. Tsiper E, Chernyak V, Tretiak S, Mukamel S. Ground-state densitymatrix algorithm for excited-state adiabatic surfaces: application to polyenes. Chem. Phys. Lett. 1999; 302:77–84.

[55]. Myers AB, Mathies RA, Tannor DJ, Heller EJ. Excited state geometry changes from preresonance raman intensities: Isoprene and hexatriene. J. Chem. Phys. 1982; 77:3857–3866.

[56]. Mukamel, S. Principles of Nonlinear Optical Spectroscopy. Oxford University Press; New York: 1995.

[57]. Thompson MJ, Bashford D, Noodleman L, Getzoff ED. Photoisomerization and proton transfer in photoactive yellow protein. J. Am. Chem. Soc. 2003; 125:8186–94. [PubMed: 12837088]

[58]. Gromov EV, Burghardt I, Köppel H, Cederbaum LS. Impact of sulfur vs oxygen on the low-lying excited states of trans-p-coumaric acid and trans-p-coumaric thio acid. J. Phys. Chem. A. 2005; 109:4623–31. [PubMed: 16833801]

[59]. Gromov EV, Burghardt I, Köppel H, Cederbaum LS. Photoinduced isomerization of the photoactive yellow protein (PYP) chromophore: interplay of two torsions, a HOOP mode and hydrogen bonding. J. Phys. Chem. A. 2011; 115:9237–48. [PubMed: 21744877]

[60]. Gonzalez EM, Guidoni L, Molteni C. Chemical and protein shifts in the spectrum of the photoactive yellow protein: a time-dependent density functional theory/molecular mechanics study. Phys. Chem. Chem. Phys. 2009; 11:4556–4563. [PubMed: 19475175]

[61]. Imamoto Y, Kataoka M, Tokunaga F. Photoreaction cycle of photoactive yellow protein from ectothiorhodospira halophila studied by low-temperature spectroscopy. Biochem. 1996; 35:14047–14053. [PubMed: 8916889]

[62]. Ren H, Biggs JD, Healion D, Mukamel S. Two-dimensional stimulated ultraviolet resonance raman spectra of tyrosine and tryptophan: A simulation study, 2012. J. Raman Spec. Submitted.

Highlights

1. We simulated 2DIR and 2D-SRR spectra of the pG and pR intermediates of PYP
2. 2DIR spectra reveal shift in amide I band
3. 2D-SRR spectra show change in cross peaks associated with chromophore C=O stretch

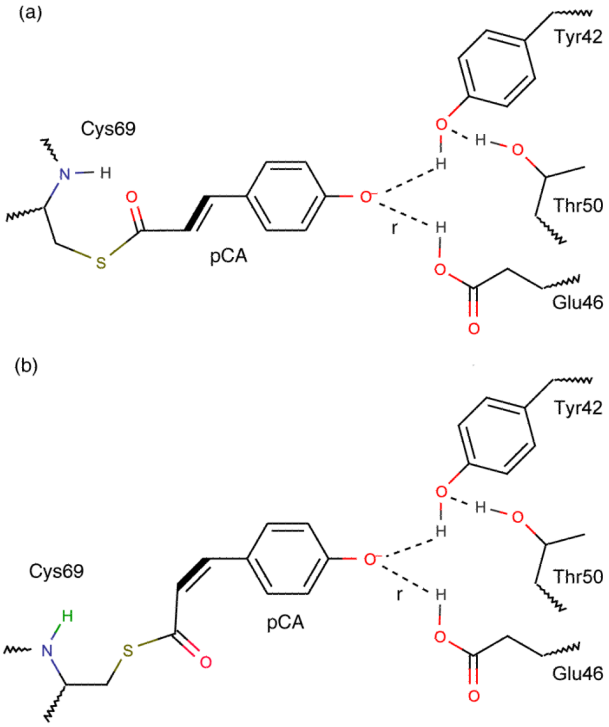

Figure 1.
Active site structure of PYP in the (a) pG and (b) pR states. Hydrogen bonds are marked in dotted lines and the Glu46(H)-pCA(O-) hydrogen bond is labeled as r. The trans to cis isomerization occurs about the pCA C=C bond and a concomitant rotation about the C-C(=O) bond breaks the hydrogen bond between pCA and Cys69.

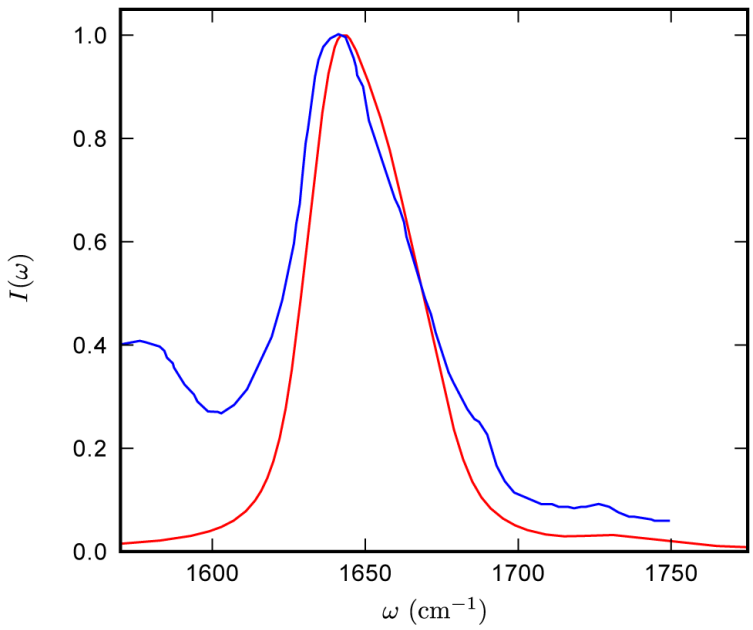

Figure 2.
Comparison of the simulated (red) and experimental (blue) [43] IR spectra of pG.

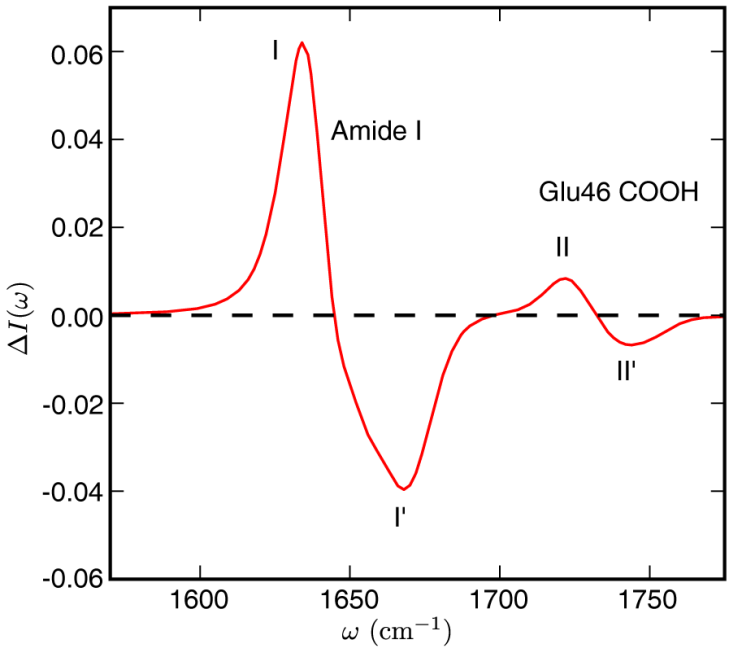

Figure 3.

The calculated difference absorption spectrum of pR and pG. The amide I region and Glu46 COOH stretching regions are clearly marked. Four peaks are labeled: (I) pR amide I, (I') pG amide I, (II) pR Glu46 COOH, and (II') pG Glu46 COOH

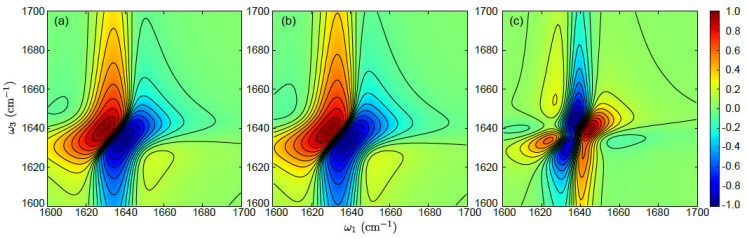

Figure 4.
The complex part of the rephasing 2D IR spectra of (a) pG and (b) pR. The difference 2D IR spectrum (pR-pG) is shown in (c).

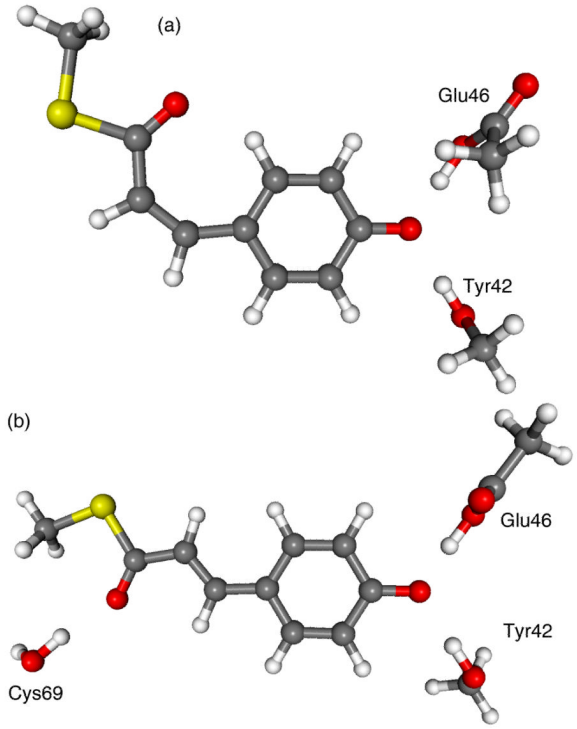

Figure 5.
The optimized ground state structures of the active site fragments of (a) pG and (b) pR used in the resonance Raman calculations.

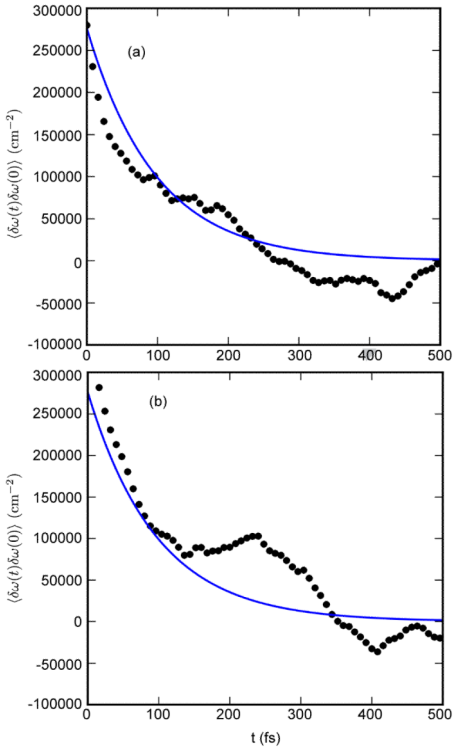

Figure 6.
The frequency-frequency correlation functions for the π-π^* excitation energy of PYP for (a) pG and (b) pR. The raw data is represented by the black dots and the exponential fit to equation 9 is represented by the blue line.

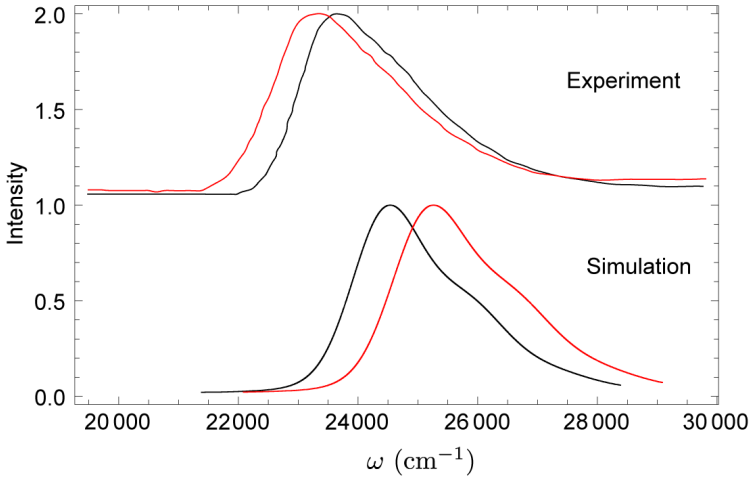

Figure 7.
Simulated (bottom) and experimental [61] (top) visible absorption spectra of PYP. The pG spectrum is shown in black and the pR spectrum is shown in red.

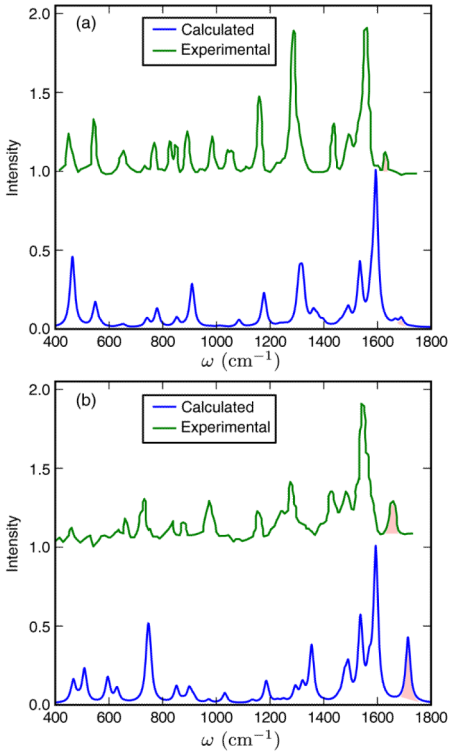

Figure 8.
Simulated (blue) and experimental [17] (green) spontaneous RR spectra for (a) pG and (b) pR.

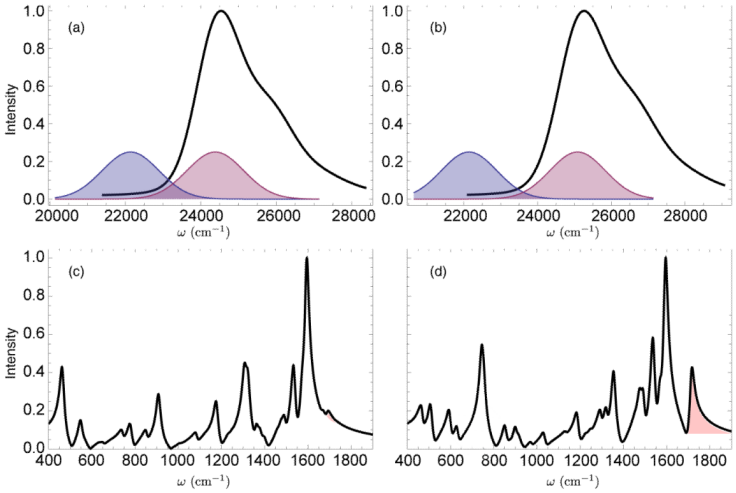

Figure 9.

1D-SRR spectra of pG and pR. The overlap of the pump (blue) and probe (magenta) pulses with the visible absorption spectra is shown in (a) pG and (b) pR. The 1D-SRR spectra are shown in (c) pG and (d) pR.

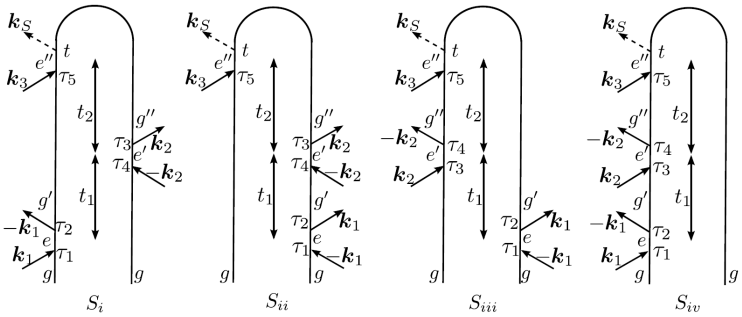

Figure 10.
The four loop diagrams used to calculate the 2D-SRR signal.

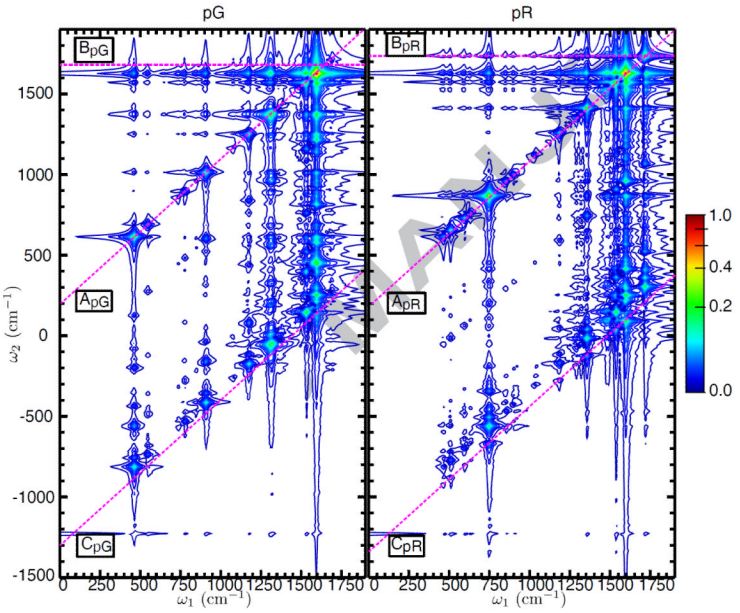

Figure 11.

Absolute value 2D-SRR spectra of (a) pG and (b) pR. Spectra were plotted on a non-linear scale arcsinh (*c*S) where S represents the signal, normalized to a maximum absolute value of 1,and $c = 10$.

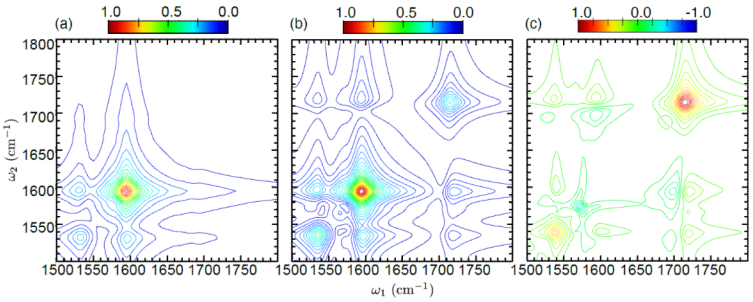

Figure 12.

Absolute value 2D-SRR spectra in the C=C and C=O stretching region for (a) pG and (b) pR. The difference 2D-SRR spectrum is shown in (c). All spectra are normalized to a maximum absolute value of 1 and are plotted on a linear scale.

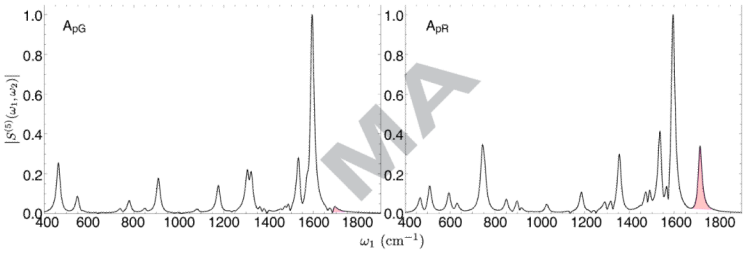

Figure 13.

The diagonal ($\omega_1 = \omega_2$) slices of the 2D-SRR spectra of (A_{pG}) pG and (A_{pR}) pR. The C=O stretching peak is shaded in pink. The labels A_{pG} and A_{pR} correspond to the labels in figure 11

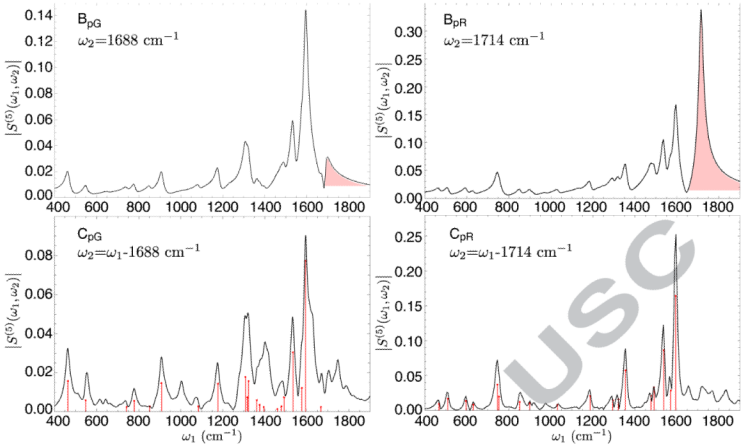

Figure 14.

The horizontal slices of the 2D-SRR spectra of (B_{pG}) pG and (B_{pR}) pR and the semi-diagonal slices associated with the pCA C=O stretch of (C_{pG}) pG and (C_{pR}) pR. The diagonal C=O stretching peak is shaded in pink in panels B_{pG} and B_{pR}. All labels correspond to the labels in figure 11

Table 1

The central frequencies and full width at half maximum (FWHM) of the Glu46 COOH peaks as estimated from the IR di erence spectrum. The FWHM is defined as $\sigma_i \sqrt{2 \ln 2}$. The average distance $\langle r \rangle$ and the standard deviation σ_r of the Glu46(H)-pCA(O^-) distance (figure 1) are also shown.

	pG	pR
ω_i (cm^{-1})	1741.86	1722.93
FWHM (cm^{-1})	26.86	18.65
$\langle r \rangle$ (Å)	3.56	1.72
σ_r (Å)	1.34	0.24

Table 2

Values of Λ, Δ, and κ obtained from the fit to equation 9 for pG and pR.

	pG	pR
Λ^{-1} (fs)	94.07	97.32
Δ (cm^{-1})	491.2	525.5
κ	0.116	0.158

Table 3

Calculated and experimental values of the frequency of maximum absorption of pG and pR in cm^{-1}.

	Calculated	Experiment
pG	24390	22472
pR	25126	21930